Chapter 6

Low Cycle Fatigue Analysis of AA6063/SiCp Metal Matrix Composites

6.1 Introduction

The low cycle fatigue (LCF) resistance of two different metal matrix composites (MMC) of AA6063 with 2% and 8% by volume silicon carbide (SiCp) particles having particulate size of 37 micron (400 mesh) at room temperature condition has been evaluated under fully reversed strain control testing. The influence of volume fraction (2 and 8 vol%) and strain ratio (R= -1) are examined. Increasing the content of SiCp results in the degradation of strain control fatigue properties while the transition fatigue life increases.

6.2 Results

Tensile tests were carried out at room temperature. Tensile engineering stress-strain curves of the as received AA6063 alloy is shown in Fig. 6.1, and for the metal matrix composites of AA6063 with 2% and 8% SiCp are shown in Figs. 6.2 and 6.3, respectively. The tensile test parameters for these cases are shown in Table 6.1 .
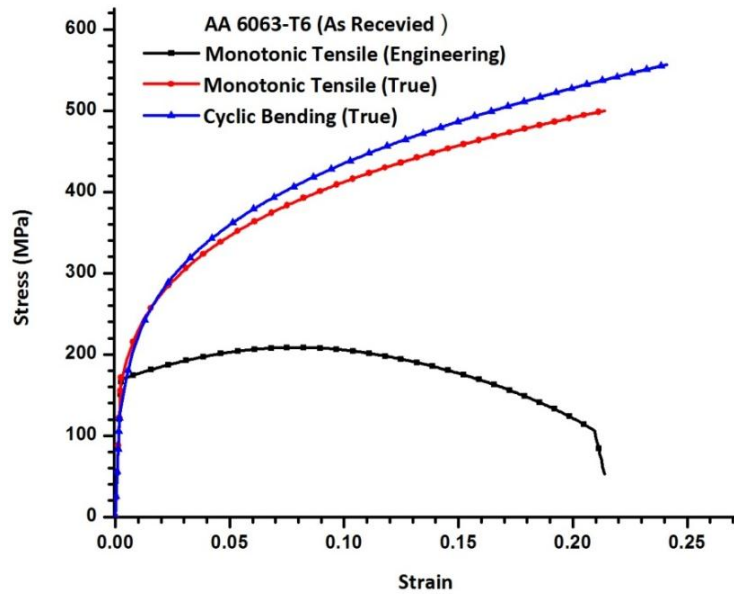
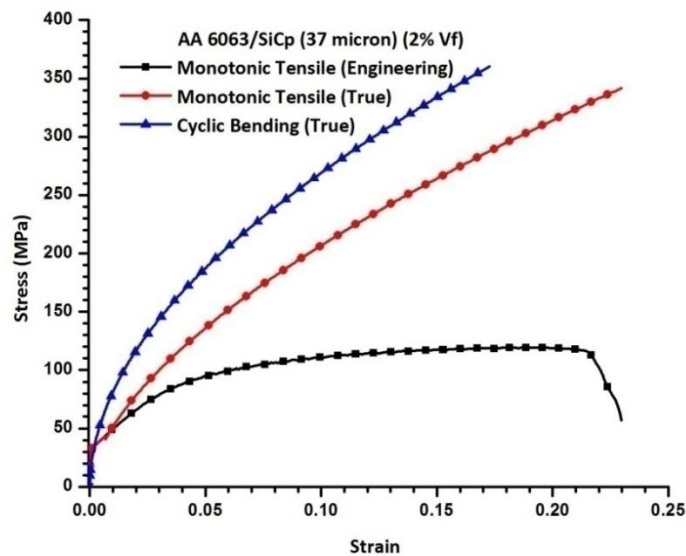**Fig. 6.1 Stress - Strain Curves for as received AA6063-T6 alloy**

Fig. 6.2 Stress-strain curves for AA6063/SiCp MMC

True plastic stress versus true plastic strain is plotted in log-log scale for the samples as shown in Fig. 6.4 and n, k values are calculated for all cases and presented in Table 6.1. Yield stresses and maximum stresses both reduce drastically for MMC cases compared to as received AA6063 case as shown in Fig. 6.5.
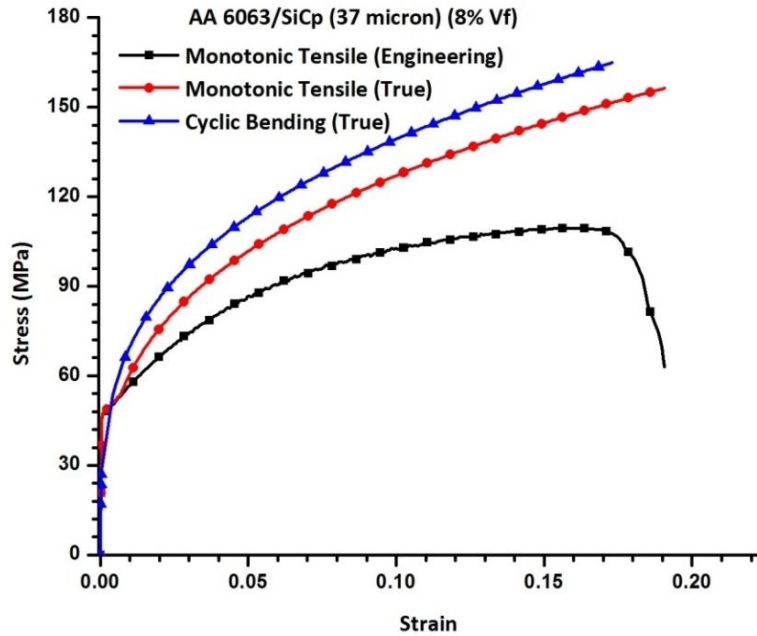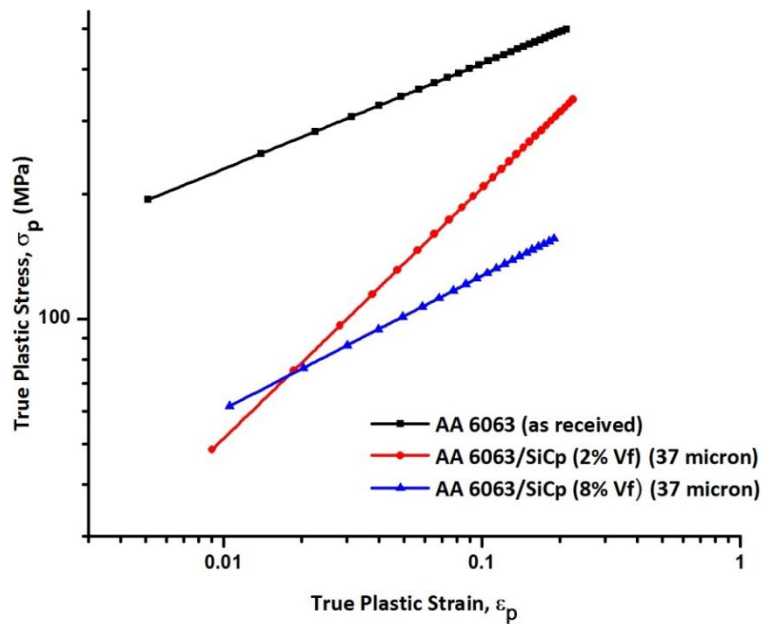
Fig. 6.3 Stress-strain curves for AA6063/SiCp MMC

Fig. 6.4 Log-Log true plastic stress versus true plastic strain plot with different volume fraction of SiCp reinforcement particle

Table 6.1 The monotonic properties of AA6063 at different volume fraction of SiCp reinforcement particle

Conditions	n	σ_f	K	$\sigma_{fracture}^{true}$	σ_y (MPa)	σ_{Max} (MPa)	$\varepsilon_{Frac.}$	E (GPa)
As Received	0.25	859.5	776.2	237.49	169.67	192.76	0.2745	68
AA6063/SiCp (2% V_f)	0.492	534.4	829.8	85.164	42.6167	118.9	0.274	72
AA6063/SiCp (8% V_f)	0.285	188.34	266.07	85.046	52.8471	126.8	0.235	75

Table 6.2 and Table 6.3 show comparison of values of n, k and $\sigma_{fracture}^{true}$ obtained experimentally for the cases AA6063/SiCp (2% V_f) and AA6063/SiCp (8% V_f), to that obtained by empirical relations given by Eqs. (2.68) to (2.70).

Table 6.2 Comparison values of n, k and $\sigma_{fracture}^{true}$ for AA6063/SiCp (2% Vf) MMC

Parameter	Experimental	Theoretical		
		Eq. (2.68)	Eq. (2.69)	Eq. (2.70)
n	0.492	0.60339	0.57146	0.49061
k	829.8	829.8	829.8	896.9
$\sigma_{fracture}^{true}$	86.164	341.5	991.8	677.26

Table 6.3 Comparison values of n, k and $\sigma_{fracture}^{true}$ for AA6063/SiCp (8% Vf) MMC

Parameter	Experimental	Theoretical		
		Eq. (2.68)	Eq. (2.69)	Eq. (2.70)
n	0.285	0.32101	0.29185	0.28574
k	266.07	266.07	266.07	312.05
$\sigma_{fracture}^{true}$	85.046	156.31	393.61	274.81

Percentage elongation decreases with increase in SiCp particle volume fraction as illustrated in Fig. 6.6. Variation of strain hardness exponent *n* and strength coefficient

K with SiCp particle volume fraction is demonstrated in Fig. 6.7. It can be observed that both n and K have a decreasing tendency.
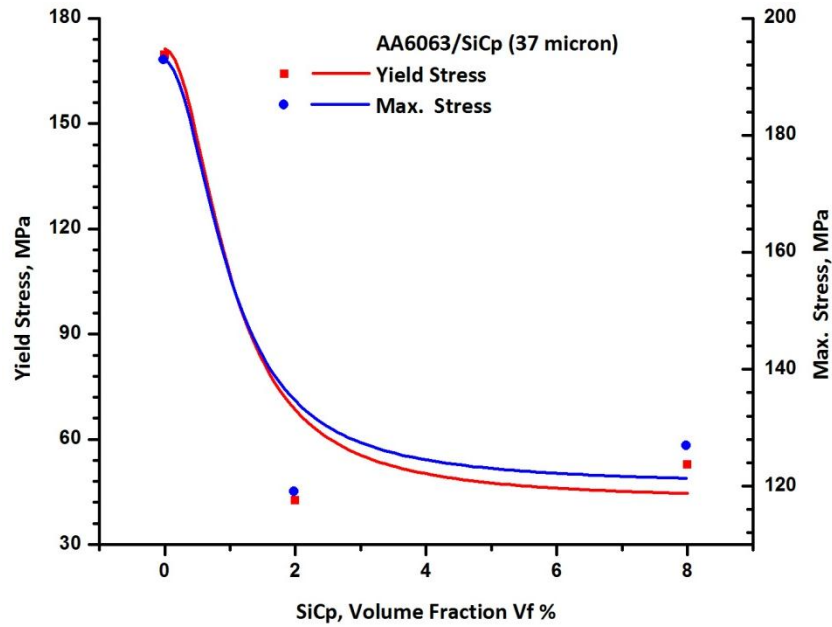

Fig. 6.5 Maximum Stress and Yield Stress variation with different volume fraction of SiCp reinforcement particle
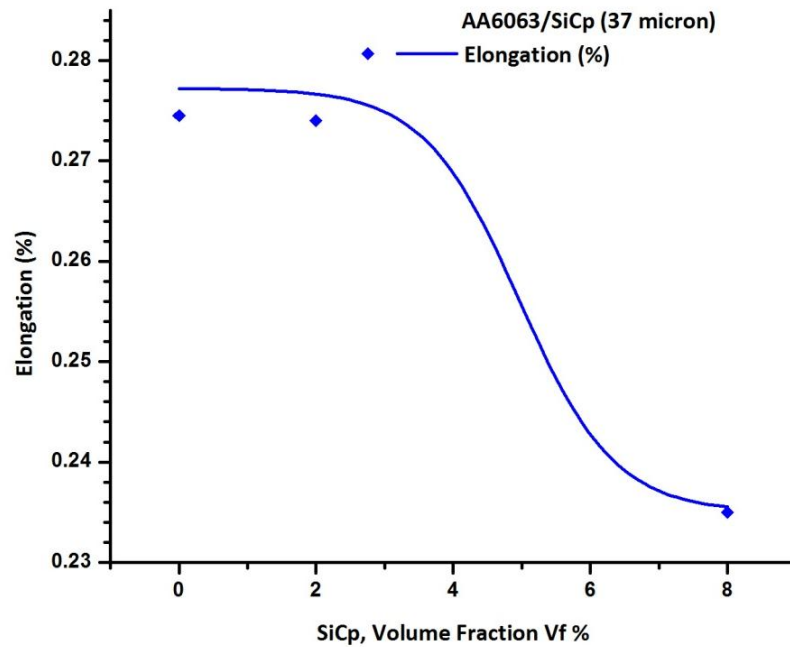

Fig. 6.6 Elongation curve variation with different volume fraction of SiCp reinforcement particle
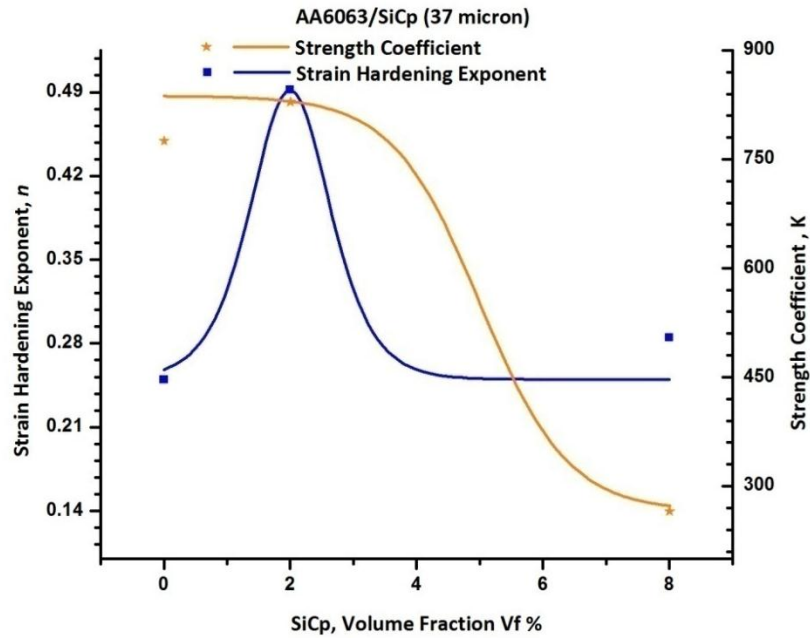
Fig. 6.7 Strength Coefficient and Strain Hardening curve variation of AA6063/SiCp with different volume fraction of reinforcement particle

Figure 6.8 shows the cyclic true bending stress-strain plots for as-received and

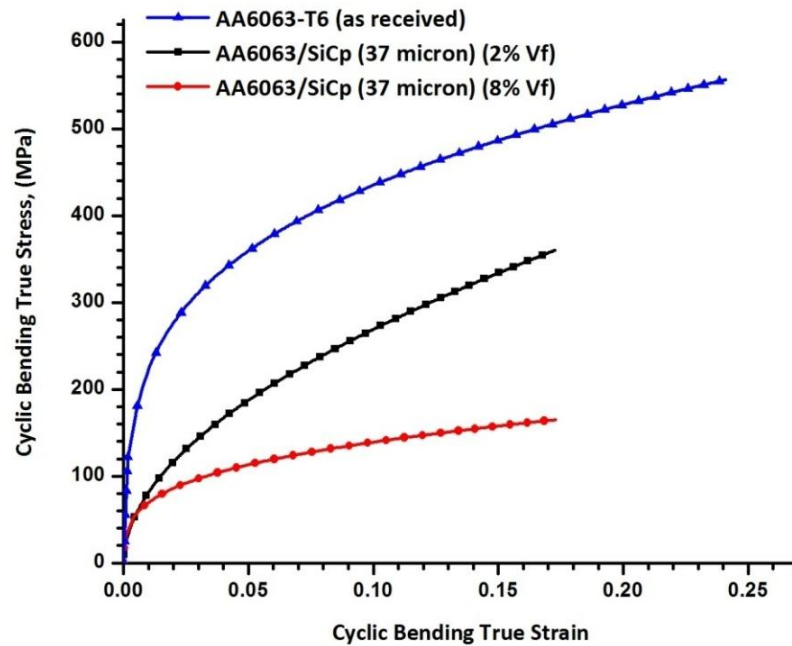two MMCs having different particulate volume fraction considered in the study.

Fig. 6.8 Cyclic Bending True Stress-Strain Curves

Torsion curves for as received AA6063, AA6063/SiCp 2% V_f MMC and AA6063/SiCp 8%V_f MMC are shown in Fig. 6.9. Different parameters obtained from torsion test are reported in Table 6.4.
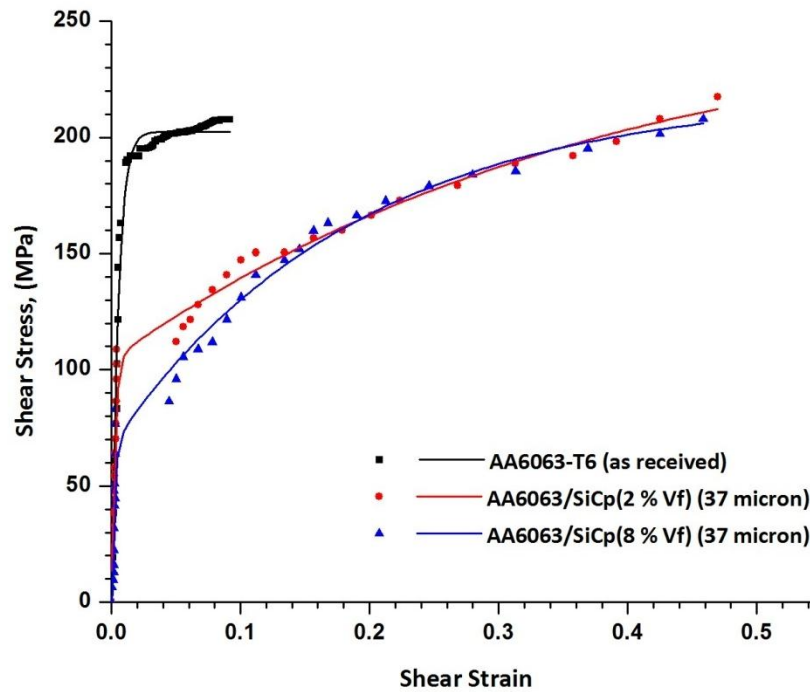

Fig. 6.9 Torsion curves

Table 6.4 Torsion test data

Parameters	Symbol	AA6063-T6 As received	AA6063 /SiCp - 2%Vf	AA6063 /SiCp - 8%Vf
Max. shear strain (Deg)	γ_{max}	6.4	5.39	26.2
Max. angle of twist (Deg)	α_{max}	100	84.165	410
Shear modulus (GPa)	G	25.9	26.8	27.5
Toughness (J/m^3)	K_t	914	5790	6490
Max. shear stress (MPa)	τ_{max}	209.03	236.6	227.026
Torque (Nm)	T_{max}	641.3	725	716.31

Figure 6.10 shows that the Maximum shear strain and Maximum angle of twist increasing with the volume fraction of SiCp particle in MMC. Variation of shear modulus and toughness with SiCp particle volume fraction are shown in Fig. 6.10. Figure 6.12 demonstrates the variation of maximum shear stress and maximum torque with SiCp particle volume fraction.
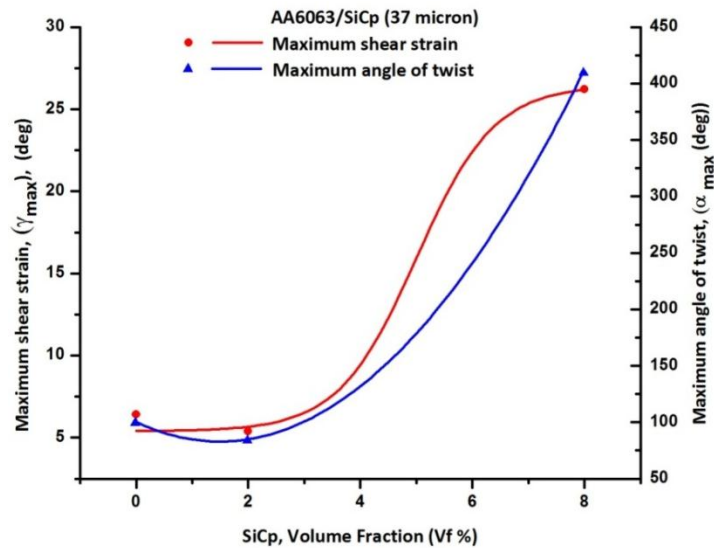

Fig. 6.9 Variation of maximum shear strain and maximum angle of twist for AA6063/SiCp with different volume fraction of reinforcement particle
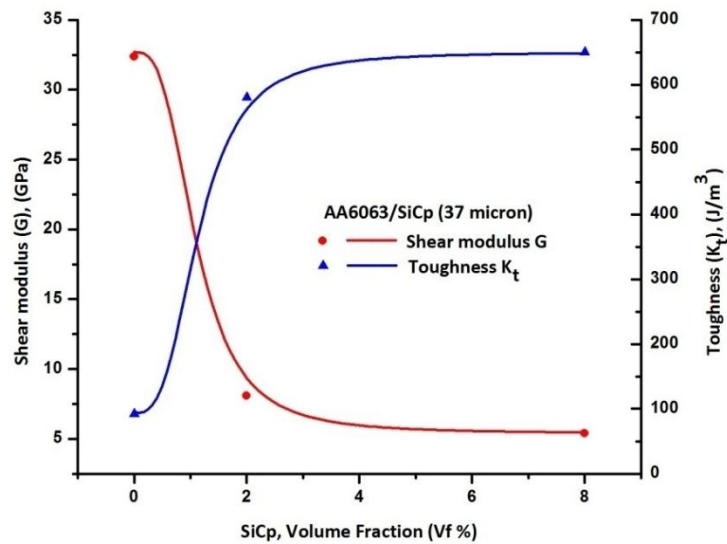

Fig. 6.10 Variation of shear modulus and toughness for AA6063/SiCp with different volume fraction of reinforcement particle
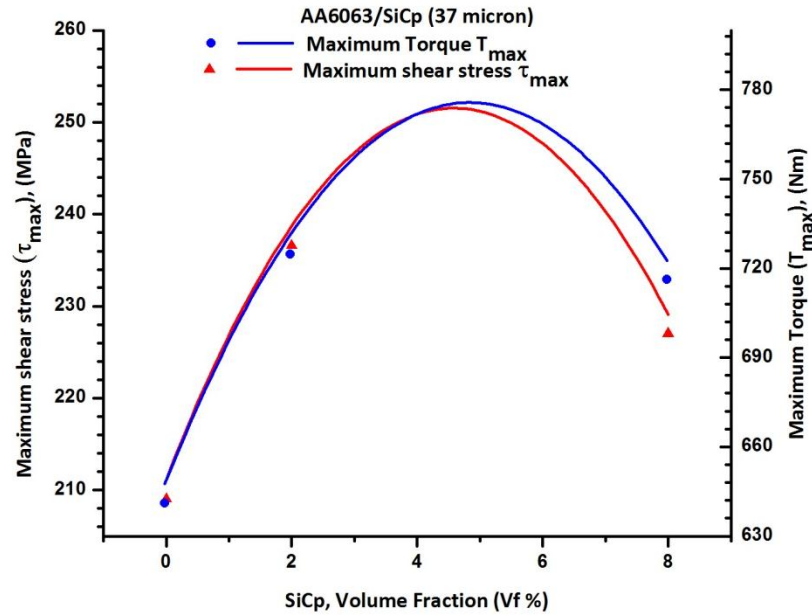
Fig. 6.11 Variation of maximum shear stress and maximum torque for AA6063/SiCp with different volume fraction of reinforcement particle

Cyclic data have been collected from the cantilever fatigue test for MMC sample having composition AA6063 with 2% by volume SiCp particles at room temperature condition and provided in Table 6.4 . The strain-life relation is plotted for this said sample and shown in Fig. 6.12. The plot illustrates elastic strain line, plastic strain line and total strain curve. The plot also shows transition fatigue life and two region viz. elastic and plastic region. In a similar way, the low cycle fatigue data for other MMC sample i.e. AA6063/8% by volume of SiCp particle is shown in Table 6.5. The strain-life relation for this case is illustrated in Fig. 6.13. The comparison of different fatigue parameters viz. ε_f', σ_f'/E, b, c, n', K' and N_T are shown in Table 6.6 for two MMC cases and as received AA6063 alloy case.

Table 6.4 Cyclic data for rotating cantilever low cycle fatigue test of AA6063/SiCp (2% V$_f$) MMC

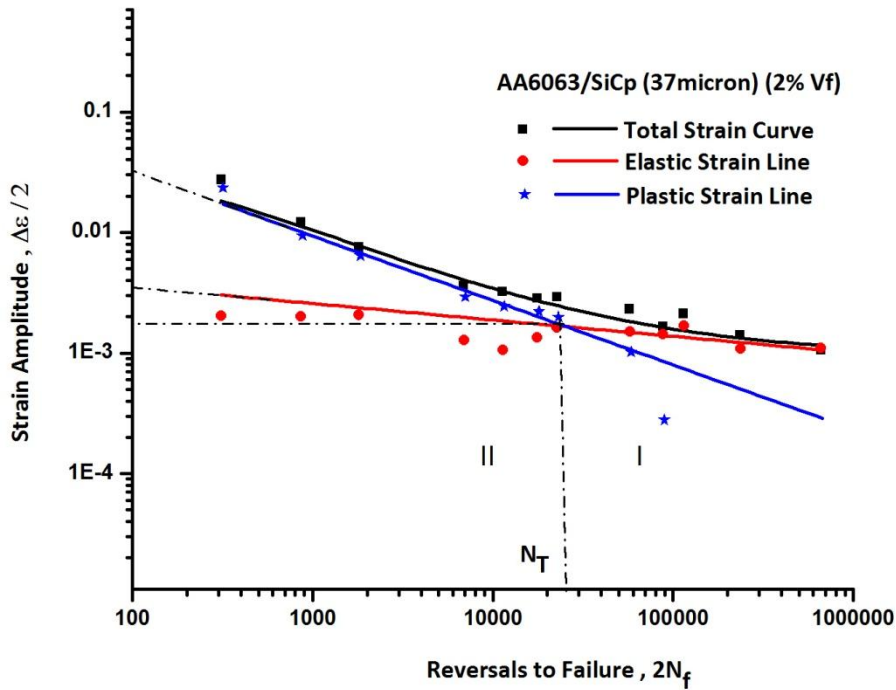| Number of cycles to failure (N$_f$)	Elastic Strain Amplitude	Plastic Strain Amplitude	Total Strain Amplitude
660757	0.001001	0.00407	0.00507
236340	0.00111	0.00521	0.00632
114593	0.00104	0.0075	0.00854
87756	0.0011	0.00841	0.00951
57303	0.00118	0.00967	0.01085
22696	0.00127	0.01128	0.01255
17650	0.00133	0.01227	0.0136
11326	0.00138	0.01326	0.01464
6900	0.00148	0.01528	0.01676
1803	0.00162	0.01839	0.02001
861	0.00177	0.02193	0.0237
311	0.00191	0.02555	0.02746

Fig. 6.12 Strain life curves for AA6063/SiCp (2% V_f) MMC

Table 6.5 Cyclic data for rotating cantilever low cycle fatigue test of AA6063/SiCp (8% V_f) MMC

| Number of cycles to failure (N_f)	Elastic Strain Amplitude	Plastic Strain Amplitude	Total Strain Amplitude
550262	8.67E-4	0.00712	0.00799
102916	9.38E-4	0.00935	0.01029
51237	9.87E-4	0.01118	0.01217
44225	0.00104	0.01351	0.01455
24655	0.00113	0.01774	0.01887
16964	0.00113	0.02305	0.02418
12365	0.00121	0.02695	0.02816
7048	0.00132	0.03088	0.0322
4672	0.00141	0.03832	0.03973
2558	0.00149	0.04681	0.0483
793	0.00155	0.05334	0.05489
310	0.00162	0.06186	0.06348
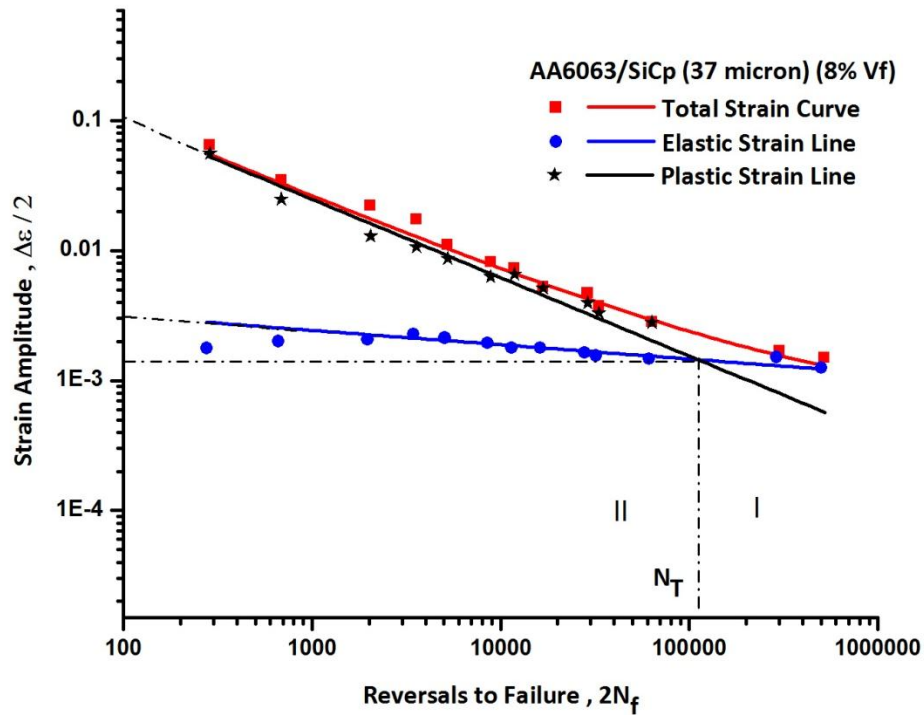
Fig. 6.13 Strain life curves for AA6063/SiCp (8% Vf) MMC

Table 6.6 Low cycle fatigue properties of aluminum alloy AA6063/SiCp with different volume fraction V_f % of reinforcement particle size

Alloy	Cyclic plastic strain (Fatigue Ductility coefficient) ε_f'	Cyclic elastic strain σ_f'/E	Fatigue Strength Coefficient σ_f' (MPa)	fatigue strength exponent b	fatigue ductility exponent c	cyclic strain hardening exponent n′	cyclic strength coefficient K′ (MPa)	transition fatigue life N_T (cycles)
As received 6063-T6	0.2915	0.006727	457.4	-0.165	-1.152	0.14322	545.7	632
6063/SiCp (2% Vf)	0.03243	0.00347	249.8	-0.079	-0.47	0.1680	444.37	25546
6063/SiCp (8% Vf)	0.112	0.00307	230.25	-0.094	-0.59	0.159	326.11	111891

Figure 6.15 elaborates total strain-life curves for as received AA6063, AA6063/2% V_f SiCp MMC and AA6063/8% V_f SiCp MMC for low cycle fatigue test. The comparison shows that MMC with 8% V_f SiCp MMC is having maximum transition

fatigue life. Figure 6.16 illustrates variation of transition fatigue life with the respect to volume % of SiCp in MMC and it is observed that the transition fatigue life increases with volume % of SiCp. Variation of fatigue strength exponent and fatigue ductility exponent with respect to volume % of SiCp are shown in Fig. 6.16.

Figure 6.18 shows variation of cyclic strain exponent and cyclic strength co-efficient with respect to volume % of SiCp reinforcement particle. Variation of cyclic plastic strain and fatigue strength co-efficient with respect to volume % of SiCp reinforcement particle is demonstrated in Fig. 6.18.
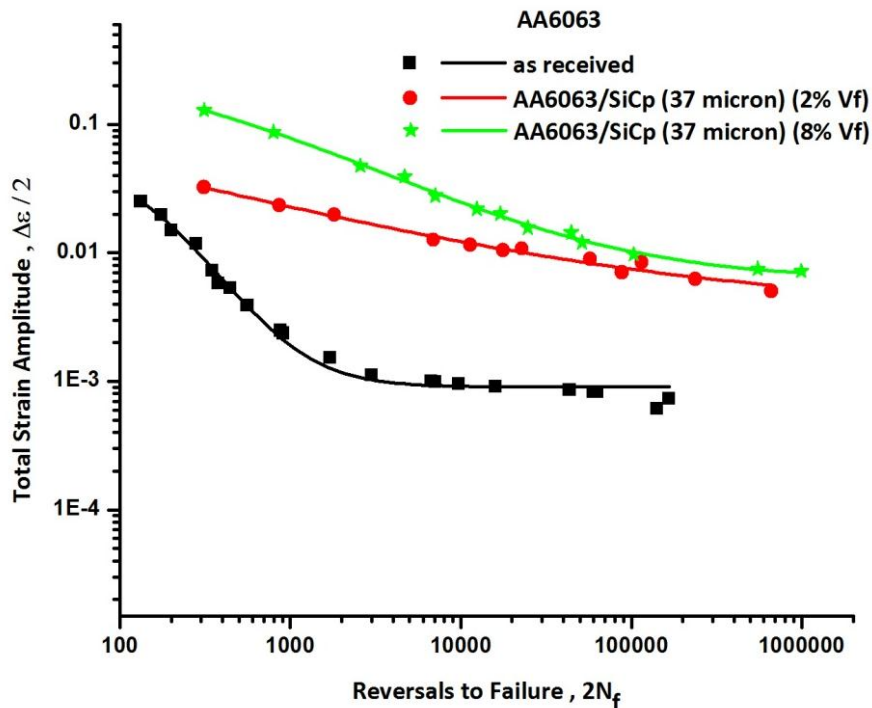
Fig. 6.14 Total strain-life curves
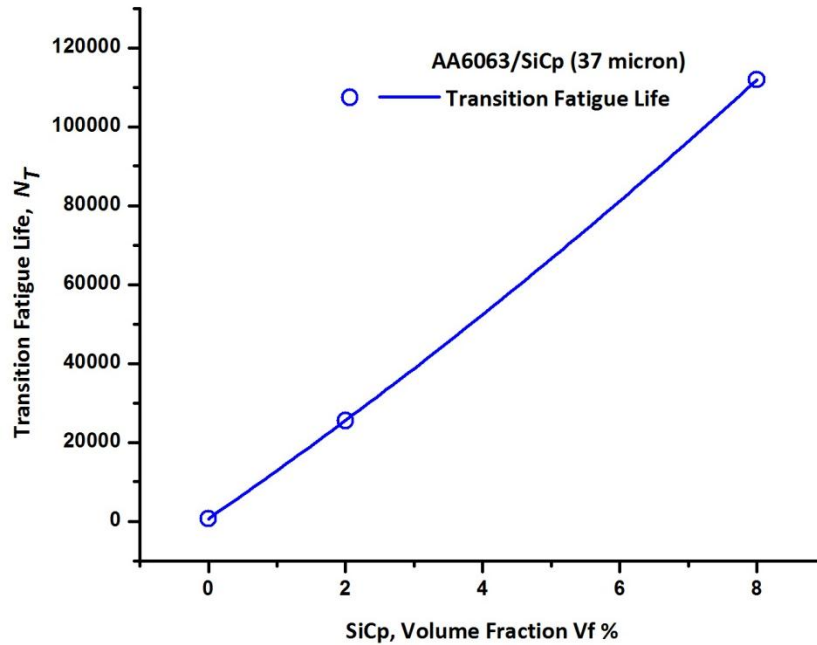
Fig. 6.15 Transition life variation with different volume fraction of SiCp reinforcement particle
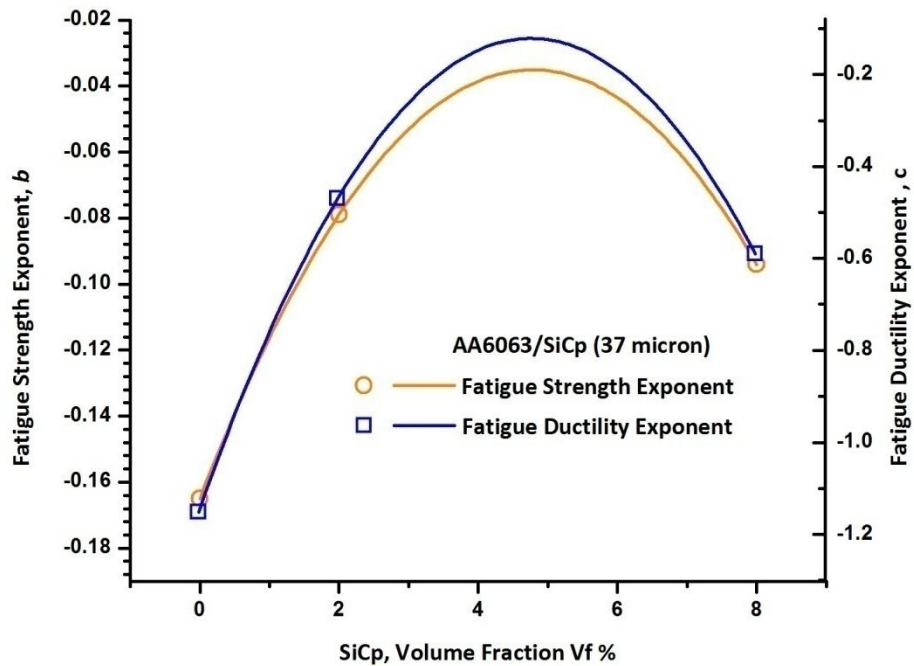

Fig. 6.16 Variation of fatigue Strength Exponent and Fatigue Ductility Exponent with different volume fraction of SiCp reinforcement particle
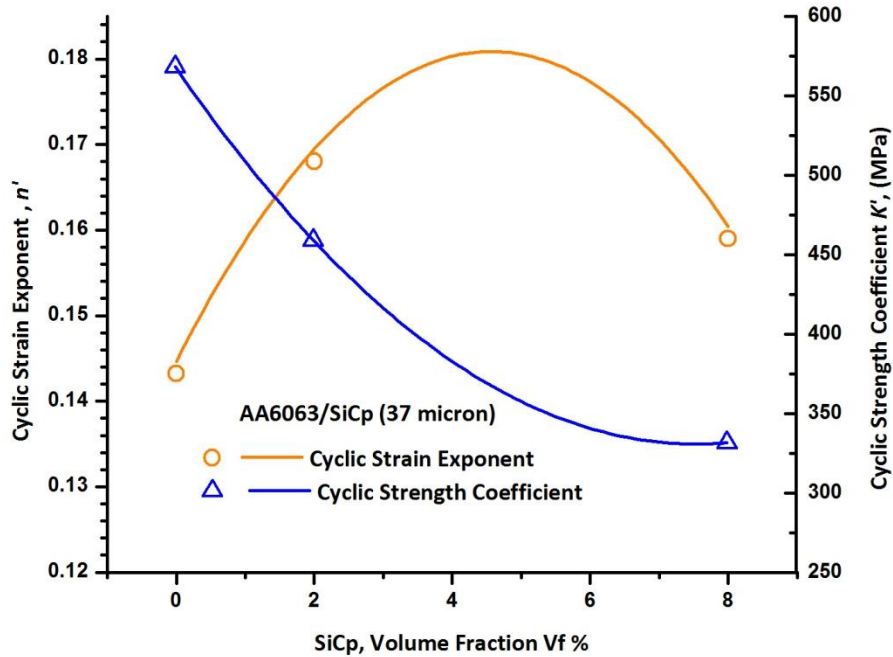
Fig. 6.17 Variation of cyclic Strain Hardening Exponent, n´ and strength coefficient K´ with different volume fraction of SiCp reinforcement particle
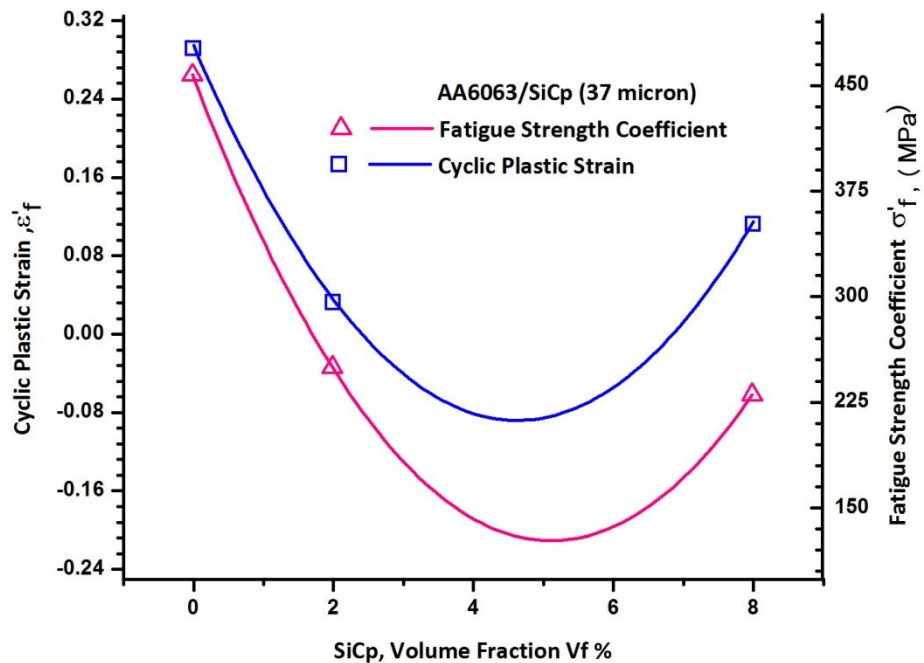

Fig. 6.18 Variation of fatigue Strength Coefficient σ'_f and cyclic plastic strain ε'_f with different volume fraction of SiCp reinforcement particle

It is also observed from Table 6.7 and Table 6.8 that empirical prediction for elastic strain is not good enough by SWT method while that of plastic strain is satisfactory. Prediction for elastic and plastic strain by Morrows method is very good.

Table 6.7 Comparison of experimental, numerical and empirical results for elastic strain AA6063 for Metal Matrix Composite at different volume fraction of SiCp reinforcement particle

Condition	Force (N)	Cycles	Elastic Strain						
			Exp.	FEM	% Diff.	SWT	% Diff.	Morrow	% Diff.
6063/SiCp 37 micron (2%Vf)	65	311	0.00191	0.0019043	0.298	0.015827	87.9	0.005497	65.25
6063/SiCp 37 micron (8%Vf)	57	310	0.00162	0.0017501	8.03	0.012714	87.25	0.004537	64.29

Table 6.8 Comparison of experimental, numerical and empirical results for Plastic strain AA6063 for Metal Matrix Composite at different volume fraction of SiCp reinforcement particle

Condition	Force (N)	Cycles	Plastic Strain						
			Exp.	FEM	% Diff.	SWT	% Diff.	Morrow	% Diff.
6063/SiCp 37 micron (2%Vf)	65	311	0.02555	0.025834	1.11	0.009473	62.924	0.00329	87.134
6063/SiCp 37 micron (8%Vf)	57	310	0.06186	0.063676	2.9	0.045206	26.922	0.016133	73.921

Figure 6.20 and Fig. 6.20 illustrate variation of elastic and plastic strains over time at a particular node on the surface of the specimen along the fracture cross-section. It is observed from the figure that plastic strain is constant over time while elastic strain varies between maximum value of 0.00196123 and minimum value of 0.00138948 for AA6063/SiCp (2% V_f) MMC and maximum value of 0.00175016 and minimum value of 0.00131551 for AA6063/SiCp (8% V_f) MMC.
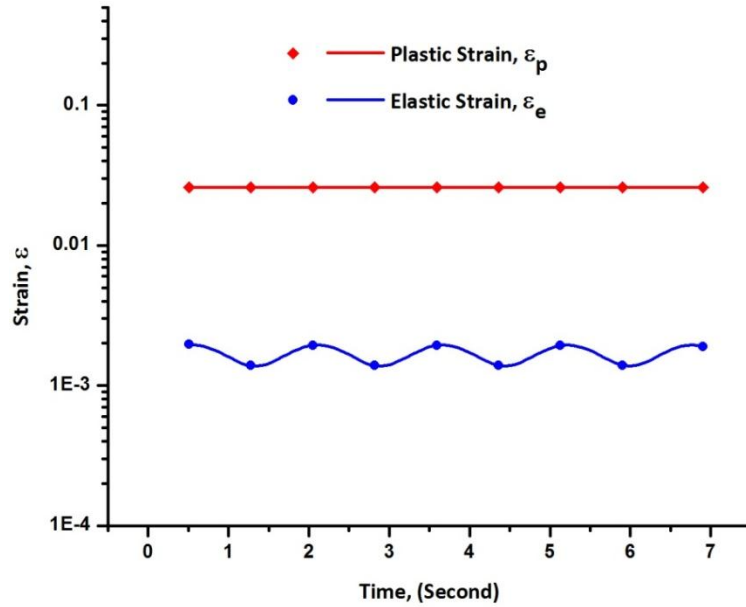
Fig. 6.19 Time history plot of elastic and plastic strain at surface node on cross section of fracture for AA6063/SiCp (2% V_f) MMC
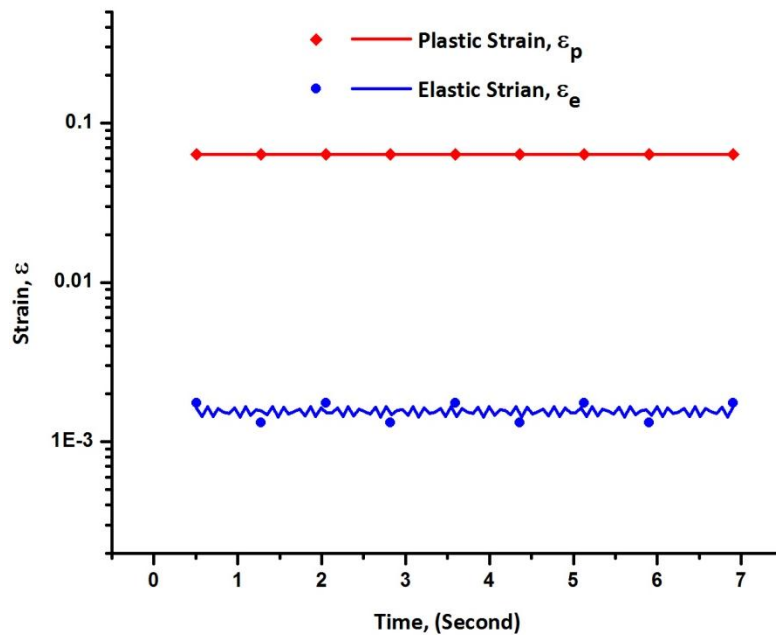

Fig. 6.20 Time history plot of elastic and plastic strain at surface node on cross section of fracture for AA6063/SiCp (8% V_f) MMC

Figures 6.22 and 6.23 show deformed shape of the specimen of AA6063/SiCp of (2% V_f) MMC at a particular instant of time with elastic and plastic strain distributions,
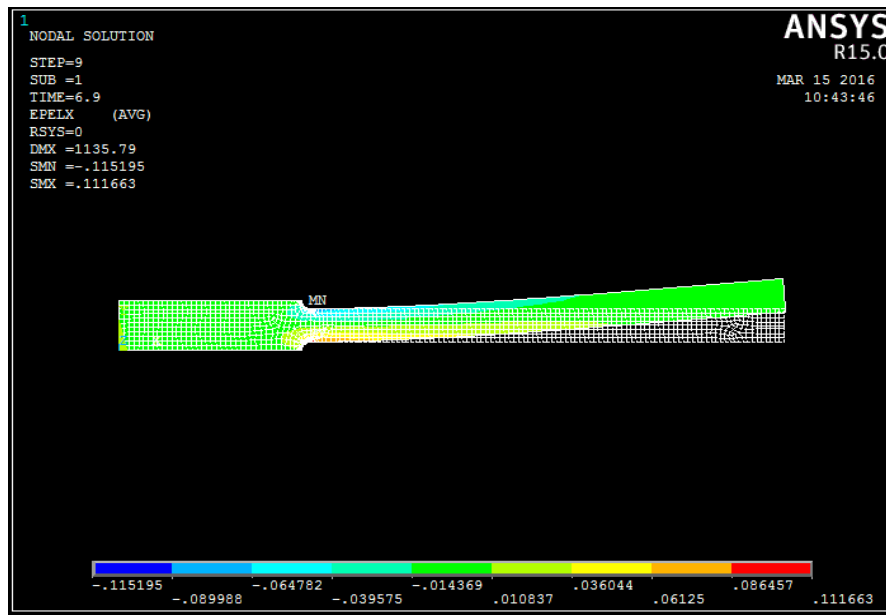
respectively. Figures 6.24 and 6.25 show deformed shape of the specimen of AA6063/SiCp (8% V_f) MMC at a particular instant of time with elastic and plastic strain distributions, respectively.

Fig. 6.21 Elastic strain at particular time on deformed shape for AA6063/SiCp of (2% V_f) MMC
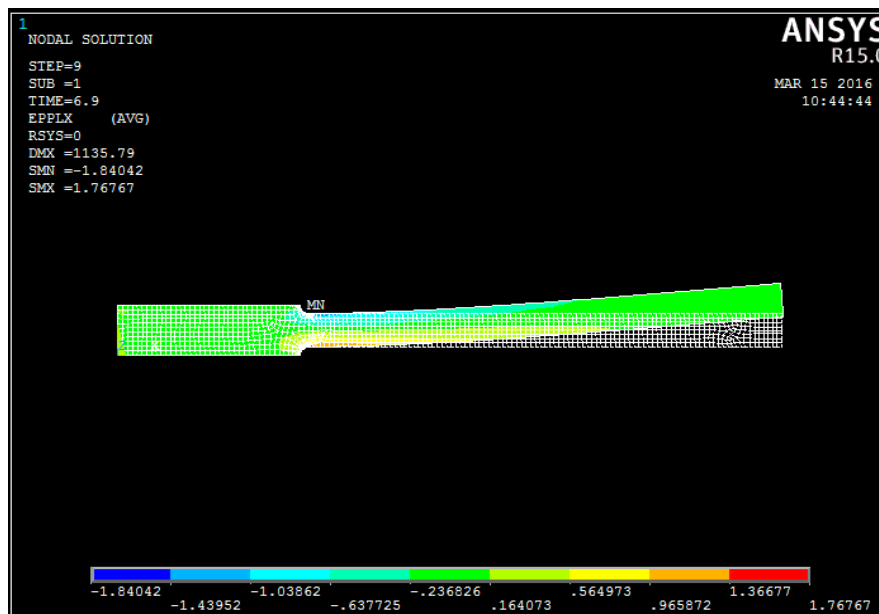

Fig. 6.22 Plastic strain at particular time on deformed shape for AA6063/SiCp (2% V_f) MMC
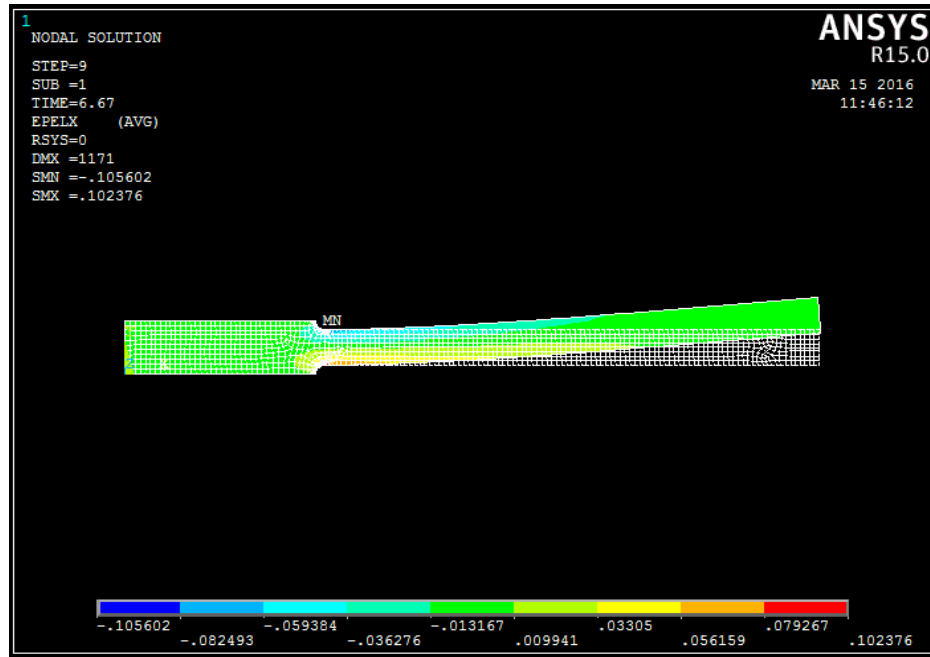
Fig. 6.23 Elastic strain at particular time on deformed shape for AA6063/SiCp (8% V$_f$) MMC
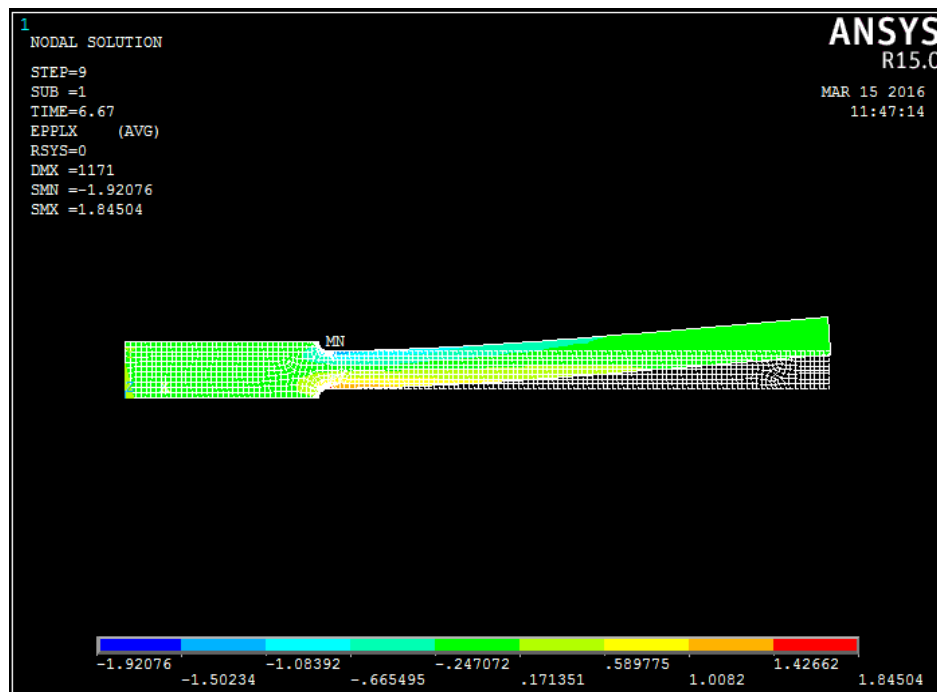

Fig. 6.24 Plastic strain at particular time on deformed shape for AA6063/SiCp (8% V$_f$) MMC

Figures 6.26 and 6.29 demonstrate fitted lines for elastic strain-life data by experimental method, least square analysis, regression for model I and model II. Different lines show good fitting as points lie evenly above and below each line for AA6063/SiCp (2% V_f) MMC and AA6063/SiCp (8% V_f) MMC, respectively. Similarly Figs. 6.27, 6.28, 6.30, 6.31 show fitting of plastic and total strain-life data experimental, least square, regression model I and model II also for AA6063/SiCp of 2% and 8% V_f of reinforcement particle, respectively. All these demonstrate that fitting by regression model II follows closely the experimental fitting. Table 6.9 shows values of R^2 and modified R^2 for elastic, plastic and total strain data.
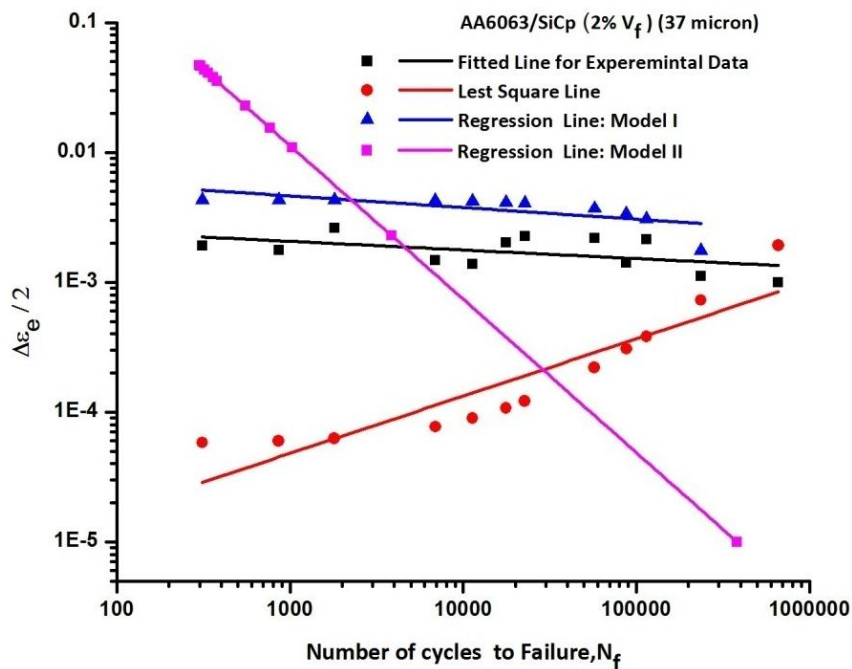

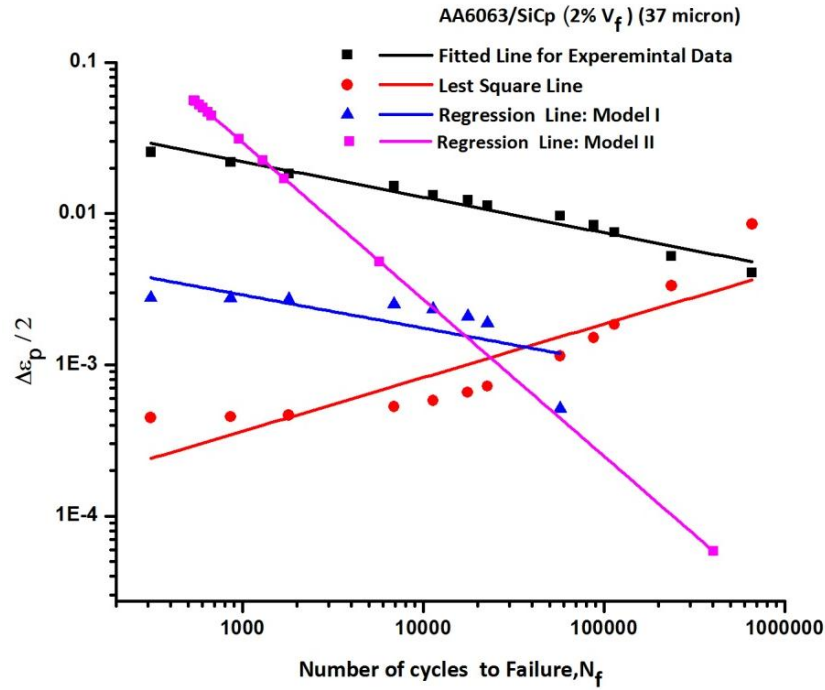**Fig. 6.25 Fitted elastic strain lines for AA6063/SiCp (2%V_f) MMC**

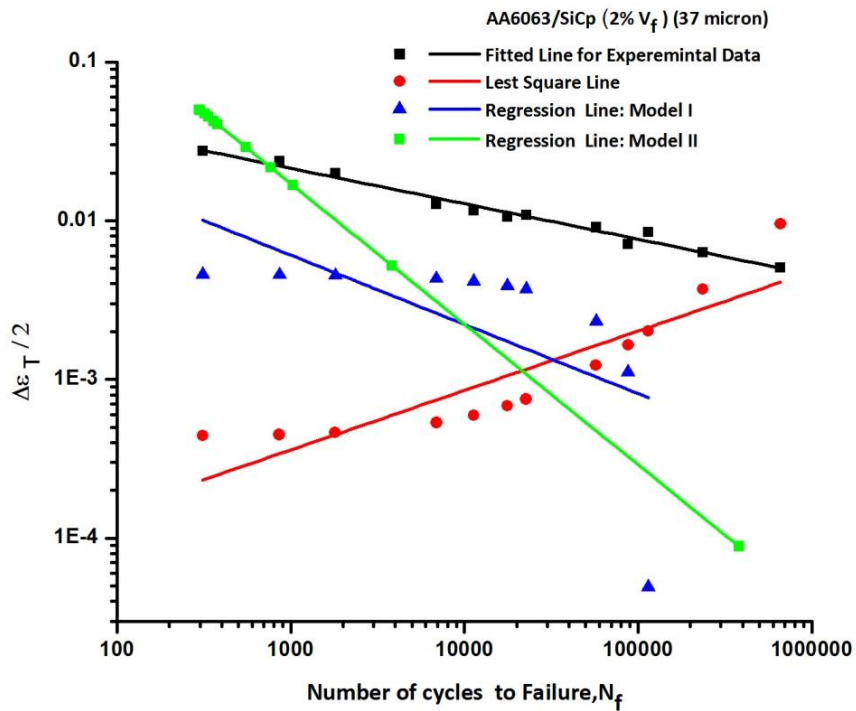**Fig. 6.26 Fitted plastic strain lines for AA6063/SiCp (2%V$_f$) MMC**

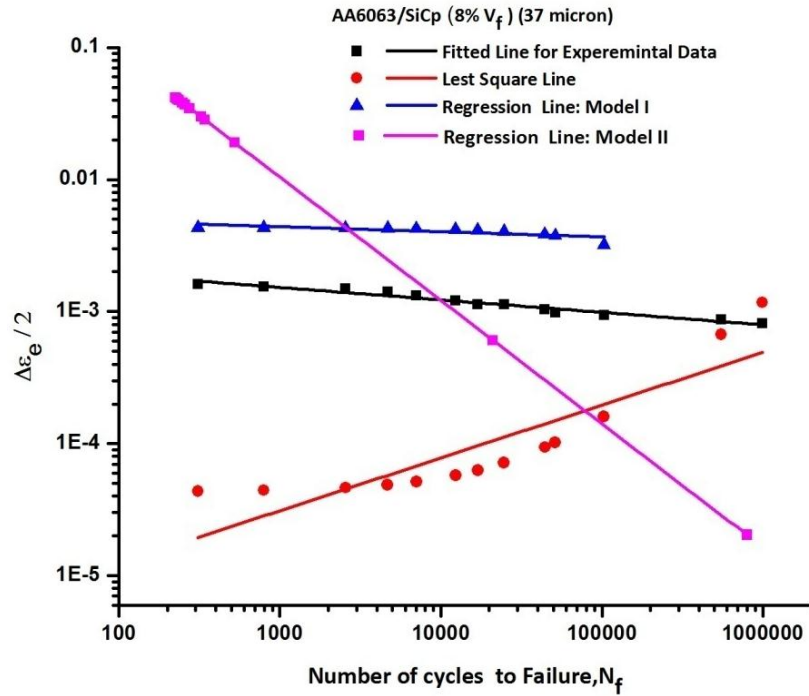**Fig. 6.27 Fitted total strain lines for AA6063/SiCp (2%V$_f$) MMC**

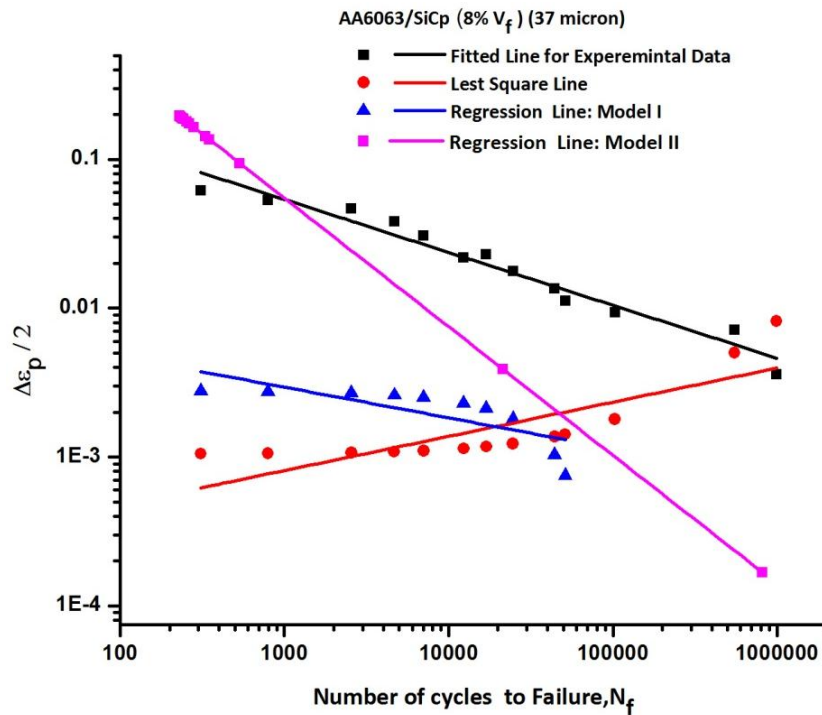**Fig. 6.28 Fitted elastic strain lines for AA6063/SiCp (8%V_f) MMC**

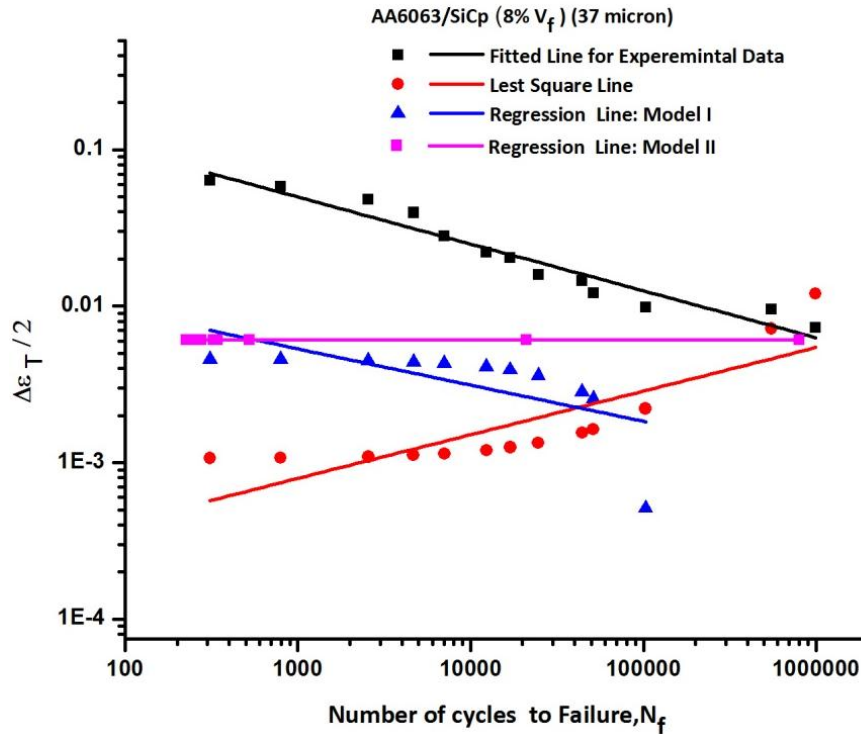**Fig. 6.29 Fitted plastic strain lines for AA6063/SiCp (8%V_f) MMC**

Fig. 6.30 Fitted total strain lines for AA6063/SiCp (8%V_f) MMC

Table 6.9 R^2 and modified R^2 values for elastic , plastic and total strain for AA6063/SiCp MMC with different volume fraction V_f of SiCp reinforcement particle

Condition	Parameters	Elastic Strain	Plastic Strain	Total Strain
AA6063-T6 as received	R^2	1.9722	0.14756	0.013728
	Mod. R^2	-3.1871	-5.1078	-5.2487
AA6063/2% SiCp (37micron)	R^2	0.001688	1.3321	0.21843
	Mod. R^2	-9.0891	-7.6377	-8.8526
AA6063/8% SiCp (37micron)	R^2	11.46	0.058529	0.11635
	Mod. R^2	2.6055	-9.9356	-9.872

Figures 6.32 to 6.33 explain how SWT parameter remains constant for AA6063/SiCp 2%

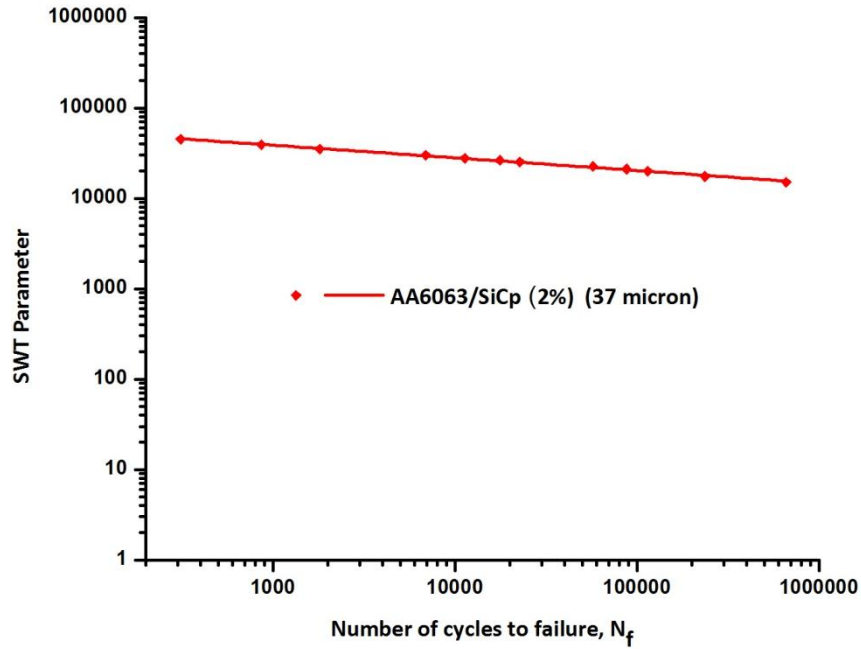and 8% V_f reinforcement particle, respectively, for rotating bending LCF data.

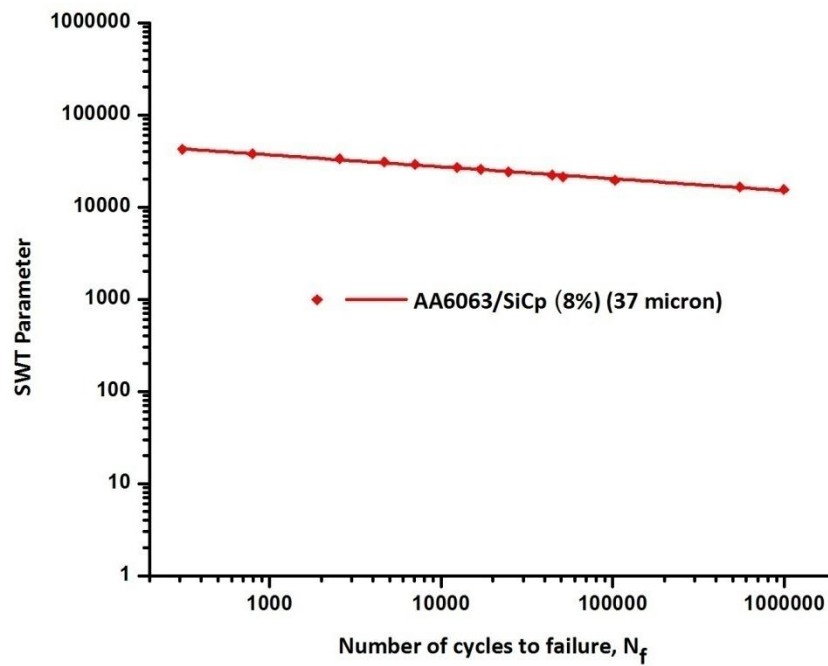**Fig. 6.31 Variation of SWT parameter with number of cycles to failure for AA6063/SiCp 2% V$_f$ MMC**

Fig. 6.32 Variation of SWT parameter with number of cycles to failure for AA6063/SiCp 8% V$_f$ MMC

6.3 Conclusions

Increasing SiCp volume percent resulted in increased fatigue life in the composites.

The addition of SiCp particles reduced the effective stress concentration on intermetallic inclusions in the matrix of the composite, increasing the fatigue life over the unreinforced alloy, where the inclusions had a higher stress concentration.

With increasing reinforcement volume fraction, yield strength decreased. With an increase in volume fraction, the number of sites for stress concentration increases, and the total amount of microplasticity also increases.